# C

# Ground Motion: Theory and Measurement

## Contents


**C.1 Introduction . . . . . 1044**
**C.2 Theory . . . . . 1044**
C.2.1 Ground Motion Spectra and Related Functions . . . . . 1045
C.2.2 The Lattice Response Function $G(k)$ . . . . . 1052
C.2.3 Combining Spatial and Frequency Dependence . . . . . 1056
**C.3 Ground Motion Measurement Devices . . . . . 1057**
C.3.1 Ground Motion Levels . . . . . 1057
C.3.2 Accelerometers . . . . . 1057
C.3.3 Geophones . . . . . 1057
C.3.4 Sensor Internal Noise Sources . . . . . 1060
C.3.5 Feedback Seismographs . . . . . 1061
C.3.6 Other New Sensors . . . . . 1063
**C.4 SLAC Ground Motion Measurements and Analysis . . . . . 1063**
C.4.1 STS-2 Measurements and Data Analysis . . . . . 1064
C.4.2 Measurement Resolution . . . . . 1064
C.4.3 Spatial Properties of the Vertical Ground Motion . . . . . 1066
C.4.4 Application to the NLC . . . . . 1069

## C.1 Introduction

One of the major challenges for the NLC will be to keep the beams stable pulse-to-pulse so the collision luminosity is not degraded. Because the beam sizes are so small, motions of the quadrupole magnets on the nanometer scale can cause significant orbit changes. Hence, the quadrupole vibration caused by the ambient ground motion is a concern as is vibration due to man-made sources, such as cooling systems.

The sensitivity to vibration depends on both the time scale and correlation of the motion. Motion slower than about 0.1 Hz will be heavily suppressed by the trajectory feedback systems in the NLC and so it is less of a concern. Motion that is random will generally be much more of a problem than motion which is correlated. For example, the tolerance on the vertical rms quadrupole motion in the linacs is 6 nm if the motion is random quad-to-quad, but orders of magnitude larger if it is correlated over distances longer than the betatron oscillation lengths of the beams.

At frequencies above 0.1 Hz, the ambient rms ground motion is generally a few hundred nm or more, but the motion is correlated over long distances. The exact nature of this correlation has a big effect on whether the resulting beam motion in an accelerator will be tolerable or not. In the past year at SLAC, we have developed both the theoretical understanding and the measurement capability to address this question for the NLC. In this Appendix, we present the results of this learning process, including measurements of both the spatial and spectral characteristics of vertical ground motion in the SLAC linac tunnel.

To begin, we develop the theoretical framework that is needed to interpret ground motion measurements and to predict its effect on beam motion. Next, we describe some of the instruments that are used to measure ground motion, including their resolutions. In the last section, we discuss the measurements that were made at SLAC, and present a model to describe the data that is based on the dynamics of wave motion in the ground. We then derive a general equation that will govern the ground-motion effect on luminosity in the NLC in the framework of this model. However, the implications for the NLC are described separately for each region of the machine in the chapters that discuss these regions.

## C.2 Theory

In this section we derive a general equation that describes the effect of ground motion on the separation of the beams at the interaction point (IP) of a collider. Specifically, we will show that the average square vertical displacement of the left-incoming from the right-incoming beam centroid can be written as an integral

$$\left\langle \Delta y_{IP}^2 \right\rangle_t = \int_0^\infty P(\omega,k)G(k)F(\omega)\frac{dk}{2\pi}\frac{d\omega}{2\pi} \tag{C.1}$$

where $<>_t$ indicates the average over time, $P(\omega,k)$ is a function describing the relevant aspects of the ground motion, $G(k)$ is a function describing the response of the lattice, and $F(\omega)$ describes the behavior of the feedback system. The definition, meaning, and properties of each of these functions are described in the next sections.

### C.2.1 Ground Motion Spectra and Related Functions

The ground displacement along the accelerator may be described by a function of two variables $y(t, s)$, where $s$ denotes position along the beam line and $t$ denotes time. To minimize any possible ambiguity, imagine that at a point to be designated as $s = 0$, a horizontal line is constructed parallel to the machine orientation and perpendicular to a radius through the origin of the earth. The variable $s$ will indicate the distance from the origin measured along this straight line. For simplicity we assume the radius of the earth at the origin of this line is chosen so the average displacement $< y(t, 0) >_t = 0$, and that $< y(t, s) >_t = 0$ for all $s$.

#### The Time Power Spectrum $P(\omega)$

A simple first question one might ask is "How large a ground displacement, at the point $s$, am I likely to experience in time $\tau$ starting from some unknown time $t$?" The answer can be given in a statistical sense as

$$\left\langle \Delta y(\tau; s)^2 \right\rangle = \left\langle [y(t + \tau, s) - y(t, s)]^2 \right\rangle \quad . \tag{C.2}$$

Assuming uniformity along the horizontal line, this should be independent of $s$, but for a local source this could conceivably be $s$-dependent. Squaring and expanding Eq. C.2:

$$\left\langle \Delta y(\tau; s)^2 \right\rangle = 2 \left[ \left\langle y(t, s)^2 \right\rangle_t - \langle y(t + \tau, s) y(t, s) \rangle_t \right] \quad . \tag{C.3}$$

The last term will be an important function for us, and we will define $P(\omega; s)$ as its Fourier transform, namely:

$$\langle y(t + \tau, s) y(t, s) \rangle_t = \int_0^\infty P(\omega; s) \cos(\omega\tau) \frac{d\omega}{2\pi} \quad . \tag{C.4}$$

The $\cos(\omega\tau)$ is appropriate because the left-hand side is unchanged by the substitution of $-\tau$ for $\tau$ (followed by the substitution of $t = t' + \tau$ and noting that the average over $t'$ is the same as the average over $t$). Next we will argue that $P(\omega) \geq 0$ for all $\omega$.

Suppose that $y(t, s)$ has been Fourier decomposed. The time average of two terms with unequal frequencies will be zero, leaving only the sum of Fourier terms times themselves shifted by the time $\tau$. That time average gives a $\cos(\omega\tau)$ times the amplitude of the term squared. The $P(\omega; s)$ must therefore be a constant times the square of a Fourier amplitude, and hence always positive.

Setting $\tau = 0$, we have the relationship

$$\left\langle y^2(t, s) \right\rangle_t = \int_0^\infty P(\omega; s) \frac{d\omega}{2\pi} \quad . \tag{C.5}$$

The quantity on the left-hand side is clearly positive for all $t$. According to the above paragraph, we can identify $P(\omega; s)$ as the contribution at frequency $\omega$ to the time averaged square of $y(t, s)$.

We will now make these statements more rigorous. Assume that we are averaging over a large time interval $[0, T]$. In this time interval, the function $y(t, s)$, for any fixed $t$, can, by imposing periodic boundary

conditions, be expanded in a Fourier series

$$\begin{aligned} y(t,s) = &\quad \textstyle\sum_{n=1}^{\infty} \left[a_n^T(s)\sin(\omega_n t) + b_n^T(s)\cos(\omega_n t)\right] \\ = &\quad \textstyle\sum_{n=1}^{\infty} c_n^T(s)\sin\left(\omega_n t + \psi_n^T(s)\right) \qquad \text{(C.6)} \\ \text{where} \qquad \omega_n = &\quad \tfrac{2\pi n}{T} \quad . \end{aligned}$$

Forming the product $y(t+\tau,s)y(t,s)$ and taking the time average (and using the orthogonality relationship of the sin and cos functions) we get

$$\langle y(t+\tau,s)y(t,s)\rangle = \sum_{n=1}^{\infty} \frac{1}{2} c_n^T(s)^2 \cos(\omega_n \tau) \quad . \qquad \text{(C.7)}$$

As $T$ gets large, this can be converted to an integral by using the relationship $dn/d\omega_n = T/2\pi$:

$$\langle y(s,t+\tau)y(s,t)\rangle = \int_0^{\infty} \frac{1}{2} \lim_{T\to\infty} \left[c_\omega^T(s)^2 T\right] \cos(\omega\tau)\frac{d\omega}{2\pi} \qquad \text{(C.8)}$$

and we can identify

$$P(\omega,s) \equiv \frac{1}{2} \lim_{T\to\infty} \left[c_\omega^T(s)^2 T\right] \qquad \text{(C.9)}$$

which is clearly a positive function for all $\omega$. Since the left-hand side of Eq. C.8 is well defined, the product $c_\omega^T(s)^2 T$ must be independent of $T$ for large enough $T$. This is equivalent to saying, that as $T$ doubles, and the number of states in a given frequency range doubles, it is the energy of the states in that region that remains constant. For this to happen, $c_n$, the amplitude of a state in the shorter time interval, must decrease as $\sqrt{2}$ in the doubled time interval. (The sum of the squares of two modes equals the square of the previously single mode.)

Thus $P(\omega;s)$ can be interpreted as the power spectrum of $y(t,s)$ at $s$. Since we will be concerned primarily with seismic sources in this appendix, we will drop the $s$ argument. We note that this $s$ independence implies that the $c_n(s)$ is also independent of $s$. Only the phase, $\psi_n(s)$, of the motion at this frequency can retain an $s$ dependence.

Since the left-hand side of Eq. C.5 is well-defined, and by experience known to be finite, the integral of the right-hand side should exist. However the left-hand side is quite large, since the daily changes in the earth's radius at any given location are about $\pm 40$ cm. In other words, though $P(\omega;s)$ is integrable, it is expected to be huge for small $\omega$. We expect that these low-frequency motions are coherent, that is to say, they are predominantly composed of long spatial wavelength motions. For these motions, the beam lines move as a whole, and we are led intuitively to believe they will not be a problem. Also there are beam-based feedback systems that receive information on beam position at 180 or 120 Hz, that will suppress the influence of low-frequency motions.

However at 0.15 Hz there is a micro-seismic peak due to ocean waves, with an amplitude as large as a micrometer, much larger than the beam spot size at the IP. To determine the impact of such motions, we must determine the wavelength decomposition of the ground motion as well as the frequency decomposition.

### The Wavelength Power Spectrum $P(k)$

Proceeding as in the previous section, one might ask: "At any given moment how much are the vertical placements at the point $s$ and $s+\ell$ likely to differ?" Again, the answer can be given in a statistical sense as

$$\left\langle \Delta y(\ell;t)^2 \right\rangle = \left\langle [y(t,s+\ell)-y(t,s)]^2 \right\rangle_s \quad . \tag{C.10}$$

Proceeding exactly as in the preceding paragraph would lead to

$$\langle y(t,s+\ell)y(t,s)\rangle_s = \int_0^\infty P(k;t)\cos(k\ell)\frac{dk}{2\pi} \tag{C.11}$$

where

$$P(k;t) \equiv \frac{1}{2} \lim_{L\to\infty} \left[c_k^L(t)^2 L\right] \tag{C.12}$$

when we analyze the motion at a fixed time $t$ along an interval in $s$ of length $L$, imposing periodic boundary conditions. $P(k;t)$ gives the wavelength power decomposition of $y(t,s)$ at time $t$. If the distance $s$ is long enough, and external conditions are not changing with $t$, we would expect this quantity to be independent of $t$, at least for short intervals of time, and we drop the explicit time-dependence, $P(k)$.

As a practical matter, when measurements are made to determine $P(k)$, the average over all $s$ is not taken. Two seismometers are placed at some $s$ separated by a distance $\ell$, and it is assumed that the average over $s$ is equal to the average over $t$, for some time interval $T$. Thus in practice we assume

$$\langle y(t,s+\ell)y(t,s)\rangle_s = \langle y(t,s+\ell)y(t,s)\rangle_t \quad . \tag{C.13}$$

### The 2D Power Spectrum $P(\omega,k)$

Because the feedback systems are operating in time (getting a piece of information at 180 or 120 Hz) the frequency of any disturbance will be of great importance. On the other hand the response of the lattice will depend on the wavelength of the disturbance, so the wavelength decomposition is of great importance. One is lead to the undeniable conclusion that one must have both, namely at each frequency one needs to know the wavelength decomposition of the motion at that frequency. One must find the answer to question, "Given two points separated by a distance $\ell$ how much does their relative vertical displacement change in time $\tau$?" This quantity is

$$\left\langle \Delta y(\tau,\ell)^2 \right\rangle = \left\langle [\{y(t+\tau,s+\ell)-y(t+\tau,s)\}-\{y(t,s+\ell)-y(t,s)\}]^2 \right\rangle_{t,s} \quad . \tag{C.14}$$

Squaring the expression within the square bracket, there are two new terms: $< y(t+\tau,s+\ell)y(t,s) >_{t,s}$ and $< y(t+\tau,s)y(t,s+\ell) >_{t,s}$. The sum of these is a symmetric function of $\tau$ and $\ell$, and as above, we can define its Fourier transform through

$$\begin{aligned} &\tfrac{1}{2}\left[\langle y(t+\tau,s+\ell)y(t,s)\rangle_{t,s} + \langle y(t+\tau,s)y(t,s+\ell)\rangle_{t,s}\right] \\ &\qquad = \int_0^\infty\int_0^\infty P(\omega,k)\cos(\omega\tau)\cos(k,\ell)\tfrac{dk}{2\pi}\tfrac{d\omega}{2\pi} \quad . \end{aligned} \tag{C.15}$$

As with P($\omega$) and P(k), P($\omega$,k) $\geq 0$ for all $\omega$ and $k$, and it is also a power spectrum.

Assume that we are averaging over a large time interval $[0,T]$ and space interval $[0,L]$. In this time and space interval the function $y(t,s)$ can be expanded in a double Fourier series

$$\begin{aligned} y(s,t) = \quad & \textstyle\sum_{m=1}^{\infty}\sum_{n=1}^{\infty}\left[a_{n,m}^{T,L}\sin(\omega_n t)\sin(k_m s) + b_{n,m}^{T,L}\sin(\omega_n t)\cos(k_m s) + \right. \\ & \left. d_{n,m}^{T,L}\cos(\omega_n t)\sin(k_m s) + e_{n,m}^{T,L}\cos(\omega_n t)\cos(k_m s)\right] \qquad \text{(C.16)} \\ & \text{where } \omega_n = \tfrac{2\pi n}{T} \text{ and } k_n = \tfrac{2\pi m}{L} \quad . \end{aligned}$$

Forming the products $y(t+\tau, s+\ell)y(t,s)$ and $y(t+\tau,s)y(t,s+\ell)$, and taking the time average (and using the orthogonality relationship of the sin and cos functions) we get

$$\begin{aligned} & \tfrac{1}{2}\left[\langle y(t+\tau,s+\ell)y(t,s)\rangle_{t,s} + \langle y(t+\tau,s)y(t,s+\ell)\rangle_{t,s}\right] \\ & \qquad = \textstyle\sum_{n,m=1}^{\infty}\tfrac{1}{4}c_{n,m}^{T,L^2}\cos(\omega_n\tau)\cos(k_m\ell) \qquad \text{(C.17)} \\ & \text{where } c_{n,m}^{T,L^2} = a_{n,m}^{T,L^2} + b_{n,m}^{T,L^2} + d_{n,m}^{T,L^2} + e_{n,m}^{T,L^2} \quad . \end{aligned}$$

As $T$ and $L$ get large this can be converted to an integral by using the relationships $dn/d\omega_n = T/2\pi$ and $dm/dk_m = L/2\pi$ and we can identify

$$P(\omega,k) = \frac{1}{4}\lim_{T,L\to\infty}\left[c_{\omega,k}^{T,L^2}TL\right] \quad . \qquad \text{(C.18)}$$

By taking $\ell = 0$ or $\tau = 0$ in the defining expression for $P(\omega,k)$, we have the following relationships among the power spectrums so far defined:

$$P(k) = \int_0^{\infty} P(\omega,k)\,\frac{d\omega}{2\pi} \quad \text{and} \quad P(\omega) = \int_0^{\infty} P(\omega,k)\,\frac{dk}{2\pi} \quad . \qquad \text{(C.19)}$$

**The Measure $\mu(\omega,k)$**

The spectrum $P(\omega)$ is observed to vary according to weather conditions and can change dramatically if there is an earthquake. Excluding earthquakes, for which we have little data, the spectrum $P(\omega)$ may change by factors of up to ten, however for any given $\omega$ the distribution of wavelengths at that frequency appears to be quite constant. This has led us to define a function $\mu(\omega,k)$:

$$\mu(\omega,k) = \frac{P(\omega,k)}{P(\omega)} \quad . \qquad \text{(C.20)}$$

The function $\mu(\omega,k)$ is a probability measure in the variable $k$, since $\int_0^{\infty}\mu(\omega,k)\frac{dk}{2\pi} = 1$ for any $\omega$. In words, $\mu(\omega,k)dk/2\pi$ gives the probability that a ground disturbance of frequency $\omega$ will contain wavelengths in the interval $dk$ about wave number $k = 2\pi/\lambda$.

If at frequency $\omega$ one has simply a wave of wavelength $\lambda(\omega)$ traveling to the right or left along the direction $s$ at velocity $v(\omega) = f\lambda = \omega/k$, then

$$\mu(\omega,k) = 2\pi\delta(k - k_0(\omega)) \quad \text{where} \quad k_0(\omega) = \frac{2\pi}{\lambda(\omega)} = \frac{\omega}{v(\omega)} \qquad \text{(C.21)}$$

and $\delta(k-k_0)$ denotes the Dirac delta function.

If at frequency $\omega$ one has only waves of wavelength $\lambda(\omega)$ traveling back and forth at some distinct angle $\theta$ to the direction $s$, then the wavelength of the disturbance along $s$ will be $\lambda_s = \lambda/\cos\theta$ and

$$\mu(\omega,k) = 2\pi\delta(k-k_0(\omega)\cos\theta) \quad \text{where} \quad k_0(\omega) = \frac{2\pi}{\lambda(\omega)} = \frac{\omega}{v(\omega)} \quad . \tag{C.22}$$

If at frequency $\omega$ one has only waves of wavelength $\lambda(\omega)$ traveling at all angles $\theta$ to the direction $s$, then there will be a distribution of wavelengths along $s$. There will be none with $k > k_0$. Since for any given angle the wave number along $s$ is $k = k_0\cos\theta$, and the distribution is presumed uniform in $0 < \theta < \pi/2$, the fraction at any $\theta$ in interval $d\theta$ will be

$$\frac{2}{\pi}d\theta = \frac{2}{\pi}dk\frac{d\theta}{dk} = \frac{2}{\pi}\frac{dk}{k_0\sin\theta} = \frac{2}{\pi}\frac{dk}{\sqrt{k_0^2-k^2}} \tag{C.23}$$

and we have

$$\mu(\omega,k) = \frac{4}{\sqrt{k_0^2(\omega)-k^2}} \quad \text{for} \quad k < k_0 \quad . \tag{C.24}$$

It is possible that at any frequency there could be contributions from several different types of waves, for example surface waves, compression waves or Raleigh waves. And there is the possibility for motion due to stochastic processes that would have an entirely different kind of behavior. For example, much discussed in the literature is a relationship called the ATL law [Baklakov 1991]. If this type of motion is present then we will show later that

$$\mu(\omega,k) = \frac{A(\omega)}{k^2} \quad \text{as} \quad k \to \infty \quad . \tag{C.25}$$

The main task of ground motion measurements will be the determination of $\mu(\omega,k)$.

### The Ratio $R(\omega,\ell)$

$P(\omega)$ gives the spectral decomposition of the rms motion of a single point. According to our definitions above

$$\left\langle y^2 \right\rangle = \int P(\omega)\frac{d\omega}{2\pi} \quad . \tag{C.26}$$

The power spectrum of the difference measurement of two points as indicated in Eq. C.10 can be written

$$\begin{aligned}
\left\langle \Delta y(\ell)^2 \right\rangle &= 2\int P(k)\,[1-\cos(k\ell)]\,\tfrac{dk}{2\pi} \\
&= 2\int\int P(\omega,k)\,[1-\cos(k\ell)]\,\tfrac{dk}{2\pi}\tfrac{d\omega}{2\pi} \\
&= 2\int P(\omega)\int \mu(\omega,k)\,[1-\cos(k\ell)]\,\tfrac{dk}{2\pi}\tfrac{d\omega}{2\pi} \\
&\equiv 2\int P(\omega)R(\omega,\ell)\tfrac{d\omega}{2\pi}
\end{aligned} \tag{C.27}$$

from which we can conclude that the power spectrum for the difference of two points separated by distance $\ell$ is related to the power spectrum of single point by the ratio 2 $R(\omega,\ell)$ with

$$R(\omega,\ell) = \int \mu(\omega,k)\,[1-\cos(k\ell)]\,\frac{dk}{2\pi} \quad . \tag{C.28}$$

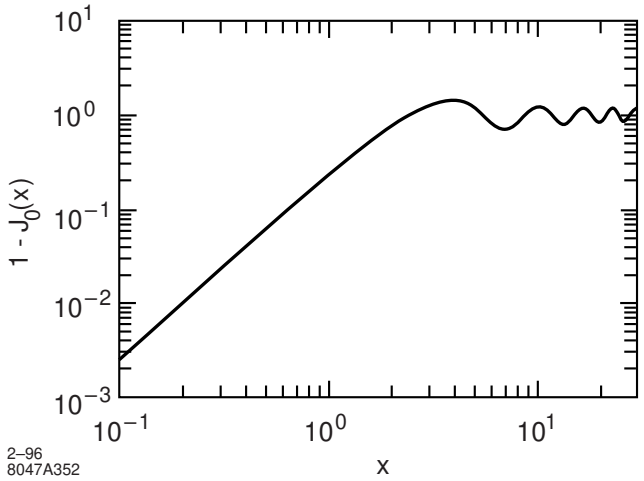


**Figure C-1.** *A log-log plot of the function $y = 1 - J_0(x)$. Note the asymptotic $x^2$ behavior for small $x$ and the position $x = 2.4$ of the intercept at which $R = 1$ ($J_0 = 0$). The first maximum is about 1.44 at $x = 3.8$.*

We are guaranteed that $R(\omega, \ell) \leq 2$.

$R(\omega, \ell)$ can be determined directly in experiments, so we must try to extract the measure $\mu(\omega, k)$ given the ratio $R(\omega, \ell)$ for many $\ell$. If one had data for many $\ell$ one could simply take a Fourier transform to find $\mu(\omega, k)$. Since we only have data at a small number of $\ell$ values, we will proceed differently by concentrating on the asymptotic behavior of $R$.

### The Ratio $R(\omega, \ell)$ as $\ell \to 0$

If the coherence of ground motion is to be helpful in suppressing its effect on beam motion, then we will be interested to know when $R(\omega, \ell)$ is small. This typically occurs as $\ell$ becomes small, so the asymptotic behavior for small $\ell$ is of special importance.

For the measure given by Eq. C.24, corresponding to waves of a single wavelength coming from all directions, then the integral of Eq. C.28 gives

$$R(\omega, \ell) = 1 - J_0\left(k_0(\omega)\ell\right) \tag{C.29}$$

where $J_0(k_0\ell)$ is the zeroth-order Bessel function. In this case, $1 - J_0(k_0 l) \to (k_0\ell/2)^2$ as $\ell \to 0$.

This asymptotic quadratic behavior is quite general for $R(\omega, \ell)$ as can be seen by looking at Eq. C.28. Suppose the measure $\mu$ has the property that

$$\overline{k^2(\omega)} \equiv \int k^2 \mu(\omega, k) \frac{dk}{2\pi} < \infty \quad . \tag{C.30}$$

Then $1 - \cos(k\ell)$ in the definition of $R$ can be expanded in a power series with the result that

$$R(\omega, \ell) \to \frac{1}{2}\overline{k^2(\omega)}\ell^2 \quad \text{as} \quad \ell \to 0 \quad . \tag{C.31}$$

This predicts a clear $l$ dependence for very general circumstances, and can be a strong consistency check on the data.

There can be other kinds of asymptotic behavior as $l \to 0$ if the second moment of $\mu$ does not exist. One such case of interest is when $\mu(\omega, k)$ has the form $A(\omega)/k^2$. In this case the condition of Eq. C.30 is not fulfilled, and the conclusion of Eq. C.31 is not valid. We will see in the next section that then $R(\omega, \ell)$ will be proportional to $\ell$ as $\ell \to 0$, which we refer to as the ATL law behavior.

### Finding the ATL Law in Ground Motion Measurements

If at a given frequency $\omega$ there is a small ATL law component together with a dominant wave motion, then its signature will be that as $\ell$ becomes small one first observes $R(\omega, \ell) \to \alpha\ell^2$, and then this behavior shifts to $R(\omega, \ell) \to \beta\ell$. In other words, on a log-log plot of $R(\omega, \ell)$ as a function of $\ell$ one should observe a change from a slope of 2 to a slope of 1. If only the $\ell^2$ behavior is seen, one can find an upper bound on the strength of the ATL coefficient. Let us suppose that this behavior is seen and for small $\ell$. Let us take

$$R(\omega, \ell) = \alpha\ell^2 + \beta\ell \quad . \tag{C.32}$$

The intersection of the two straight-line behaviors will occur at $\ell = \ell_x$ with $\ell_x = \beta/\alpha$. The value of $R$ at this intersection will be $R(\omega, \ell) = 2\beta^2/\alpha$, twice the value of the extension of either straight line. If no departure from an $\ell^2$ behavior can be seen, we can conclude that $\ell_x (= \beta/\alpha) < \ell_{min}$, where $\ell_{min}$ is the smallest $\ell$ for which data is available. Hence $\beta < \alpha\ell_{min}$. We will use this relationship to establish upper bounds on the magnitude of the ATL law coefficient. Now we show how this asymptotic behavior is related to the measure $\mu(\omega, k)$.

Suppose that $\mu(\omega, k)$ has a $1/k^2$ tail. This is allowed because $dk/k^2$ is integrable as $k \to \infty$. Let us decompose the measure into two parts, one which contains the $1/k^2$ tail, and another which possesses a second moment. We write $\mu = \mu_R + \mu_T$ and take

$$\mu_T(\omega, k) = \frac{a(\omega)}{k^2}\left[1 - e^{-\frac{k^2}{2k_1^2}}\right] \tag{C.33}$$

where $k_1$ is a cut-off parameter.

The measure $\mu_T$ contains the $1/k^2$ tail and is integrable at both large and small $k$. The integral of the measure (integrate by parts) gives the fraction of the measure which is in the tail:

$$\mu_T(\omega) \equiv \int_0^\infty \mu_T(\omega, k)\frac{dk}{2\pi} = \frac{1}{2\sqrt{2\pi}}\frac{a(\omega)}{k_1(\omega)} \quad . \tag{C.34}$$

$\mu_R = \mu - \mu_T$ is supposed to have a finite second moment. Hence for small $\ell$

$$\begin{aligned} R(\omega, \ell) &= \int (\mu_R + \mu_T)\left[1 - \cos(k\ell)\right]\tfrac{dk}{2\pi} \\ &\to \tfrac{\ell^2}{2}\int \mu_R k^2 \tfrac{dk}{2\pi} + \int \mu_T\left[1 - \cos(k\ell)\right]\tfrac{dk}{2\pi} \\ &= \tfrac{\ell^2}{2}\left\langle k^2 \right\rangle_R + \tfrac{a(\omega)}{4}\ell - \tfrac{\ell^2}{4}\tfrac{a(\omega)k_1}{\sqrt{2\pi}} \\ &= \tfrac{\ell^2}{2}\left[\left\langle k^2 \right\rangle_R - \mu_T(\omega)k_1^2\right] + \tfrac{a(\omega)}{4}\ell \quad . \end{aligned} \tag{C.35}$$

The coefficient $A$ in the ATL law results in a spectral coefficient $4A/(k^2\omega^2)$. Hence the relation between $A$ and $a(\omega)$ is given by

$$A = \omega^2 P(\omega)\frac{a(\omega)}{4} \quad . \tag{C.36}$$

Typically $A$ is thought to be in the range of $10^{-4} < A < 10^{-6}\,\mu\mathrm{m}^2/\,\mathrm{m/s}$. If there is no evidence of linear $\ell$ behavior, we can place a limit on $A$ of $\omega^2 P(\omega)\beta < \omega^2 P(\omega)\alpha\ell_{\min} = \omega^2 P(\omega)\alpha\ell_{\min}$ where $\alpha$ is the coefficient of the $\ell^2$ behavior and $\ell_{\min}$ is the smallest $\ell$ in the data set.

We note in closing that mathematically other behaviors at small $\ell$ are allowed, of the form $\ell^\epsilon$ with $0 < \epsilon \leq 2$, corresponding to tail behaviors of $1/k^{1+\epsilon}$.

## C.2.2 The Lattice Response Function $G(k)$

### Sum Rules for Optical Functions

We will suppose that we have a lattice of elements with the quadrupole strength, $\kappa(s)$, given as a function of $s$. This function is defined by

$$\kappa(s) = \frac{B_T(s)}{a(s)(B\rho)} \tag{C.37}$$

where $B_T(s)$ is the quadrupole pole-tip field at $s$, and $a(s)$ is the radius of the pole tip. $B\rho = p/q$ is the particle momentum divided by the charge.

We will assume that there is some ideal line along which the magnets are arranged, and the displacement is given as a function of time by $y(t,s)$ with $< y(t,s) >_t = 0$. Then the displacement of the beam at the end of the beam line, which we will denote by $s = 0$, is

$$y_B(t) = \int_0^L \kappa(s)y(t,s)R_{34}(s)ds + R_{33}(L)y(t,L) \quad . \tag{C.38}$$

The assumption here is that the beam enters the beam line at a displacement equal to the ground level. It will be the function of the upstream beam line to carry out this task. Any failure to do this can be accounted for by calculating the deviation due to the upstream beam line and multiplying by $R_{33}(L)$. We will define a quantity $\Delta y_B(t)$ which is the difference $y_B(t) - y(t,0)$. Then

$$\Delta y_B(t) = \int_0^L \kappa(s)y(t,s)R_{34}(s)ds + R_{33}(L)y(t,L) - y(t,0) \quad . \tag{C.39}$$

If one translates the beam line by inserting a $y(t,s)$ which is independent of $s$, then $\Delta y_B(t)$ should be zero. According to Eq. C.39 this requires that

$$0 = \int_0^L \kappa(s)R_{34}(s)ds + R_{33}(L) - 1 \quad . \tag{C.40}$$

This is true, because $R_{34}(s)$ from $s \to 0$ is the same as the $R_{34}$ from $0 \to s$. The latter is a sine-like ray coming from the origin, which we will denote by $\tilde{y}$ and has $\tilde{y}'(0) = -1$. Because of the equations of motion

$\kappa(s)\tilde{y}(s) = \tilde{y}''(s)$, the integral in Eq. C.40 is $\tilde{y}'(L) - \tilde{y}'(0)$. The derivative of the $R_{34}$ function coming from the origin is just $-1$ times the $R_{44}$ function coming from the origin, which equals the $-1$ times the $R_{33}$ function going from $s$ to the origin. Hence Eq. C.40 is found to be valid, as it must.

If one inserts $y(t,s) = \alpha s$ into Eq. C.39, then $\Delta y_B(t)$ should again be zero if $L$ is $n\pi$ from the origin. (If the phase change from 0 to $L$ equals $n\pi$, the slope of the incoming beam does not affect the position at the IP). This implies that

$$0 = \int_0^L s\kappa(s)R_{34}(s)ds + LR_{33}(L) \quad . \tag{C.41}$$

Inserting $\tilde{y}(s)$ for $R_{34}$, substituting $\kappa(s)\tilde{y}(s) = \tilde{y}''(s)$ as above, and integrating by parts, and using the fact that $\tilde{y}(L) = 0$, one can confirm Eq. C.41.

These intuitively valid relationships would imply that it is not the magnitude of a displacement, nor even its slope that will cause beams not to collide, but it is the curvature of the earth's displacement that is important.

We have gone into some detail to describe and confirm these optical rules, because often approximations used for optical functions do not satisfy these conditions, and numerically incorrect results are obtained. A high degree of suppression of motion will only be obtained numerically when these sum rules are obeyed.

### Paired Lattices

For lattices that have the property that for every $-I$ section there is an identical $-I$ section adjacent to it, which we designate as a "paired lattice," we have the result that if the displacement function has constant curvature the effects of the two adjacent sections will cancel one another. This leads to the conclusion that for paired lattices it is not the displacement, the slope, or the curvature, but the derivative of the curvature that causes a displacement of the beam.

### Definition of $G(k)$

We will first write the beam displacement from the ground motion at the IP as a sum,

$$\Delta y_B(t) = \sum \mu_i y(t, s_i) \tag{C.42}$$

where the $\mu_i$ are dimensionless numbers equal to $\kappa(s_i)R_{34}(s_i)\Delta s_i$ or $R_{33}(L)$ or $-1$. Now we square this to get

$$\begin{aligned} < \Delta y_B(t)^2 > &= \textstyle\sum_{i,j} \mu_i\mu_j < y(t,s_i)y(t,s_j) >_t \\ &= \textstyle\sum_{i,j} \mu_i\mu_j \int_0^\infty P(k)\cos[k(s_i - s_j)]\frac{dk}{2\pi} \\ &= \textstyle\int_0^\infty P(k)\frac{dk}{2\pi}\sum_{i,j}\mu_i\mu_j\cos[k(s_i-s_j)] \\ &= \textstyle\int_0^\infty P(k)\frac{dk}{2\pi}\left[\left(\sum_i \mu_i\cos ks_i\right)^2 + \left(\sum_i \mu_i \sin ks_i\right)^2\right] \\ &\equiv \textstyle\int_0^\infty P(k)G(k)\frac{dk}{2\pi} \quad . \end{aligned} \tag{C.43}$$

The lattice properties are completely contained in the sum, and therefore we have defined a lattice response function $G(k)$ by

$$G(k) = \left(\sum_i \mu_i \cos ks_i\right)^2 + \left(\sum_i \mu_i \sin ks_i\right)^2 \quad . \tag{C.44}$$

It is precisely $\Delta y_B^2$ for a cosine wave plus $\Delta y_B^2$ for a sine wave.

We note that in the special case were we are looking at the displacement of the two beams from one another at the IP, then if we assume that the NLC is symmetric, the cosine wave gives no displacement of the two beams, and the sine wave effect is doubled. Hence, when considering the effect on luminosity due to ground motion in both halves of a symmetric NLC, we have

$$G(k) = 4\left(\sum_i \mu_i \sin ks_i\right)^2 \tag{C.45}$$

where the sum is only over one half of the machine.

**Behavior of $G(k)$ as $k \to 0$**

As $k \to 0$, $\cos(ks_i) \to 1$. As shown above the constant term can give no net displacement. The next term is $1/2k^2s_i^2$. This term has a constant curvature, so for a paired lattice it will also be zero. The first term surviving from the cosine sum squared will go as $k^8$ in this case.

As $k \to 0$, $\sin(ks_i) \to ks_i$. As shown above the constant slope term also gives no net displacement. The first term surviving from the sine sum squared will go as $k^6$.

Some examples of $G(k)$ for various lattice sections are shown in Figures C-2, C-3, and C-4.

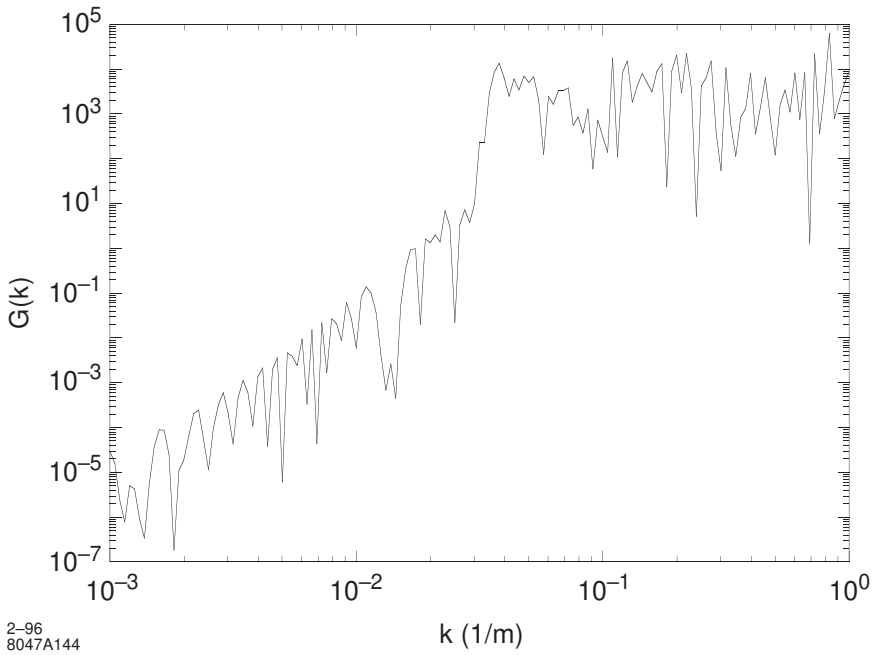


**Figure C-2.** *NLC-IIb linac lattice response function assuming symmetric linacs (i.e., Eq. C.45) that are separated by 10 km.*

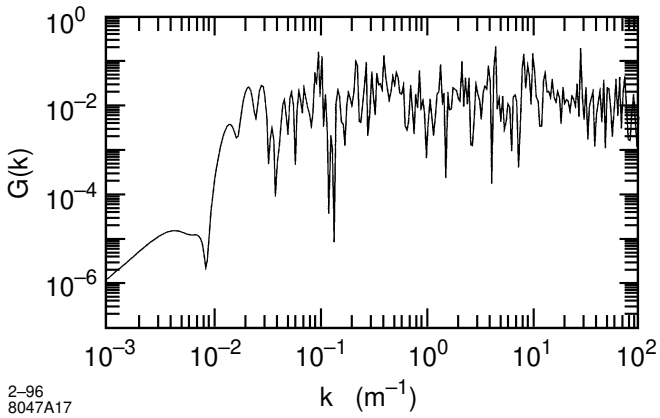


**Figure C-3.** *Collimation system lattice response function.*

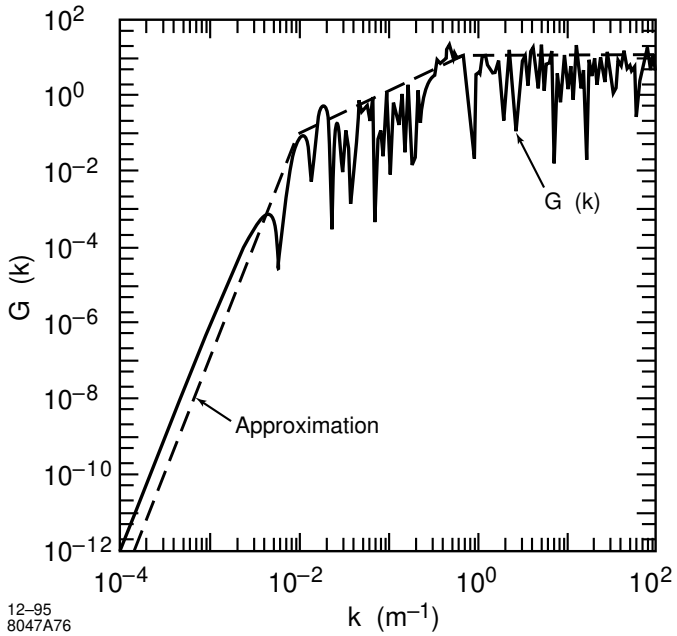


**Figure C-4.** *Final-focus lattice response function.*

### C.2.3 Combining Spatial and Frequency Dependence

$F(\omega)$

The particulars of a feedback response function will vary according to the exact feedback algorithm employed. In each case however there is a function $F(\omega)$ which will give the effect of the feedback for each input frequencies. As a result Eq. C.43 can be generalized, in the presence of feedback, to be

$$< \Delta y_B(t)^2 >_t = \int P(\omega,k)G(k)F(\omega)\frac{dk}{2\pi}\frac{d\omega}{2\pi} \quad . \tag{C.46}$$

$G_\mu(\omega)$

Once the measure $\mu(\omega,k)$ has been determined, $P(\omega,k)$ in Eq. C.46 can be replaced by $P(\omega,k) = P(\omega)\mu(\omega,k)$ and the integral over $k$ in Eq. C.46 can be carried out. The result of doing the $k$ integral we will denote by

$$G_\mu(\omega) \equiv \int_0^\infty \mu(\omega,k)G(k)\frac{dk}{2\pi} \quad . \tag{C.47}$$

This gives the response of the lattice to the combination of wavelengths present in the ground motion at the frequency $\omega$. Doing this integral first, Eq. C.46 becomes

$$\left\langle \Delta y_B(t)^2 \right\rangle_t = \int_0^\infty P(\omega)G_\mu(\omega)F(\omega)\frac{d\omega}{2\pi} \quad . \tag{C.48}$$

# C.3 Ground Motion Measurement Devices

## C.3.1 Ground Motion Levels

Seismic ground noise varies greatly with time and place. Down to about 1 Hz, a large variety of instrument types can resolve ground noise at noisy sites where cultural noise dominates the spectrum. At the quietest sites though, only the most sophisticated instruments have broad enough bandwidth and a low enough noise floor to accurately measure ground motion from 0.1 Hz to 100 Hz. An informal ground noise standard has been developed at the USGS for bench marking seismic instruments. The power spectral densities for ground noise at some of the most quiet sites in North America have been averaged into a low-noise model which is now included in the instrument noise-floor plots of the most sensitive commercial instruments. Figure C-5 shows the acceleration and displacement amplitude spectra for this low-noise model.

These plots show that at 1 Hz the seismic instrument must detect nano 'g's of acceleration per $\sqrt{\text{Hz}}$ which corresponds to 1/10ths of nanometers of ground displacement per $\sqrt{\text{Hz}}$. Ground motion at most accelerator sites is 10 to 100 times larger than the low-noise model for frequencies $\geq$1 Hz where cultural noise dominates.

## C.3.2 Accelerometers

The simplest, least expensive detectors are piezoelectric crystals coupled to sensitive charge amplifiers. These instruments are high-sensitivity versions of industrial machine vibration detectors. Their frequency response is nearly flat up to the first resonance of the crystal (100 Hz–1000 Hz). Their noise floor is dominated by electrical noise in the high-gain pre-amp. Figure C-6 shows information from the data sheet for the Wilcoxon Model 731 piezoelectric seismic accelerometer.

At 1 Hz, noise in the Model 731 is equivalent to an acceleration spectral density of 50 ng/$\sqrt{\text{Hz}}$ or a displacement density of 13 nm/$\sqrt{\text{Hz}}$. For noisy sites this detector might show ground noise signals above self-noise at frequencies above 5 Hz, but it does not reach the low-noise model noise floor at any frequency. Its most useful application is the direct measurement of local sources of mechanical noise such as cooling system flow turbulence and pulsed power conversion equipment.

## C.3.3 Geophones

Moving coil velocity meters or geophones transduce earth motion by electromagnetic induction. Figure C-7 shows a simple geophone model. They contain a permanent magnet and a moving coil attached to a spring suspended mass. A voltage is produced across the coil that equals the transduction ($G$) times the relative velocity ($\dot{x} - \dot{x}_g$) of the mass measured with respect to the permanent magnet which is fixed in the housing of the transducer.

A typical geophone suitable for microseismic ground motion studies is the L4C Geophone made by Mark Products. The 1-kg-proof mass and suspension system has a 1-Hz resonant frequency. In addition to its intrinsic internal mechanical damping, this instrument is usually brought to a .707 critically damped response by shunting the output by a damping resistor $R_s = 8905\Omega$. The Laplace transform transfer function of output

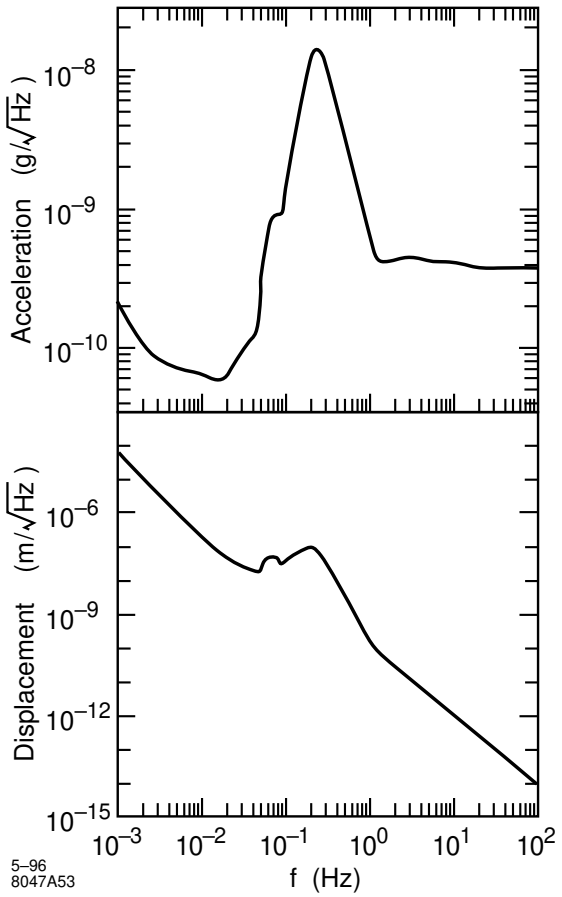


**Figure C-5.** *USGS low-noise model.*

voltage *vs.* input ground velocity is:

$$\frac{V_{\rm out}(s)}{\dot{x}_g(s)} = \frac{R_s}{R_c + R_s} G \left( \frac{s^2}{s^2 + 2\omega_0 \zeta s + \omega_0^2} \right) \quad \text{where} \quad 2\omega_0 \zeta = \left( b + \frac{G^2}{R_c + R_s} \right) / M \quad . \tag{C.49}$$

The amplitude and phase of the complex function $V_{\rm out}(i\omega)/\dot{x}_g(i\omega)$ are plotted in Figure C-8. Above resonance ($s >> i\omega_0$), the transducer conversion factor from Table C-1 for a damped L4C geophone is:

$$\frac{V_{\rm out}}{\dot{x}_g} = \frac{8905\ \Omega}{5500\Omega + 8905\Omega} (276.4\,{\rm V\,s/\,m}) = 170.9\,{\rm V\,s/\,m} \quad . \tag{C.50}$$

One-nm rms motion at 10 Hz, for example, would produce a 11-$\mu$V signal at the geophone's output if a 8905-$\Omega$ external damping resistor is used.

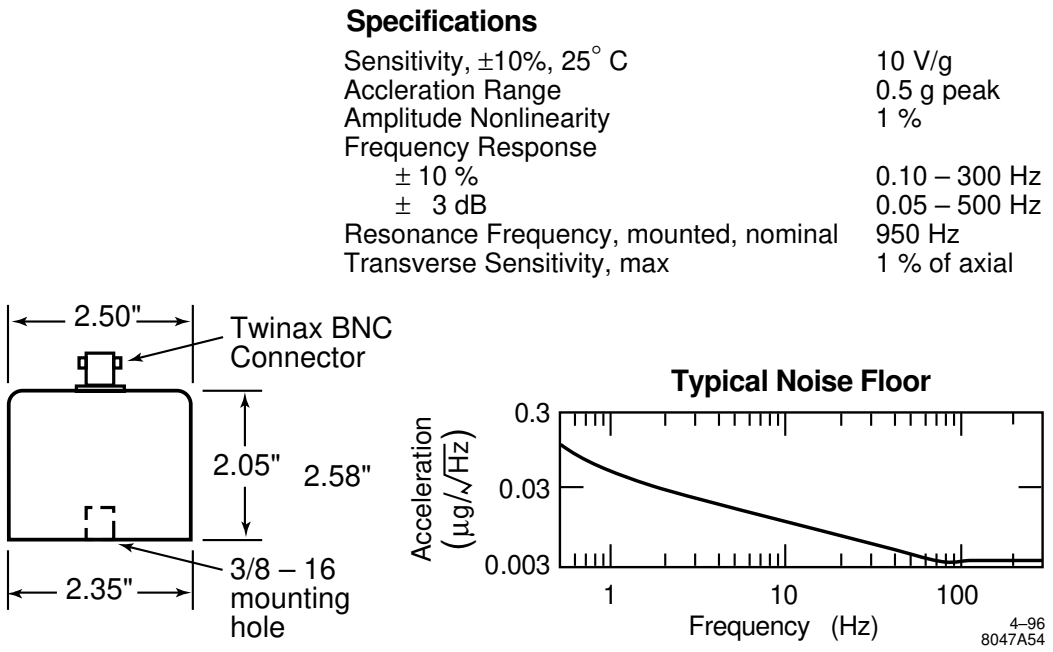


**Figure C-6.** *Wilcoxon Model 731 accelerometer specifications.*

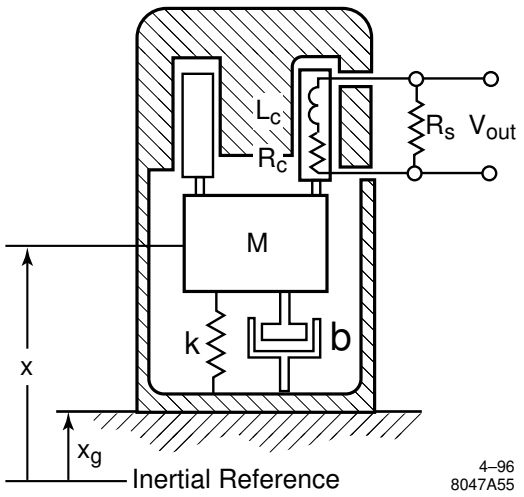


**Figure C-7.** *Geophone Model.*

| | | | |
|---|---|---|---|
| Transduction | G | 276.4 | V s/m |
| Natural Frequency | $\omega_0$ | $2\pi$ | rad/s |
| Coil Resistance | $R_c$ | 5500 | $\Omega$ |
| Shunt Resistance | $R_s$ | 8905 | $\Omega$ |
| Damping | $\zeta$ | .707 | |

**Table C-1.** *L4C parameters.*

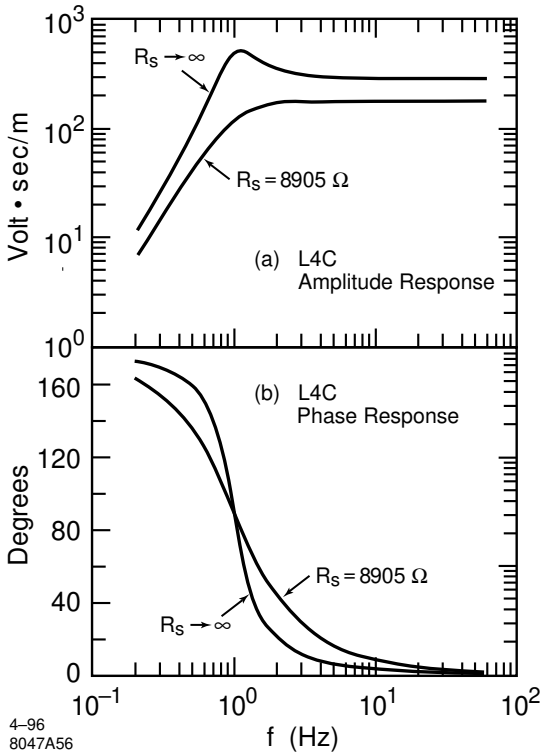


**Figure C-8.** *L4C transfer function.*

### C.3.4 Sensor Internal Noise Sources

All inertial instruments sense the relative motion of a proof mass with respect to ground. There are three major sources of instrument noise: Brownian motion of the proof mass which is in thermal equilibrium with the outside world through various damping mechanisms [Gabrielson 1993], Johnson noise in the sensor output circuit and electrical current and voltage noise in the input amplifier [Rodgers 1992, Riedesel 1990]. Thermal noise in the mechanical proof mass/suspension system depends on the damping ratio $\zeta$ and the ratio of resonant frequency to proof mass. The power spectral density of acceleration noise above resonance is

$$S_{\rm mech} = 16\pi kT\frac{\zeta f_0}{M} \quad ({\rm m/s^2})^2/\,{\rm Hz} \quad . \tag{C.51}$$

For a .707 critically-damped 1-Hz oscillator with a 1-kg mass at room temperature, $S_{\rm mech}$ is $1.46\times10^{-19}({\rm m/\,s^2})^2/\,{\rm Hz}$. Integrating the corresponding displacement density above one Hz yields 6-picometer rms motion. For comparison, the low-noise model integrates to 60-picometer rms above 1 Hz. While thermal mechanical noise is not a serious limit for large proof masses with critical damping, it does set a limit for smaller sensors with proof masses measured in grams.

Johnson noise in the sensor output circuit generates a white-noise voltage signal:

$$S_{\rm johnson} = 4kTR \quad ({\rm V^2/\,Hz}) \quad . \tag{C.52}$$

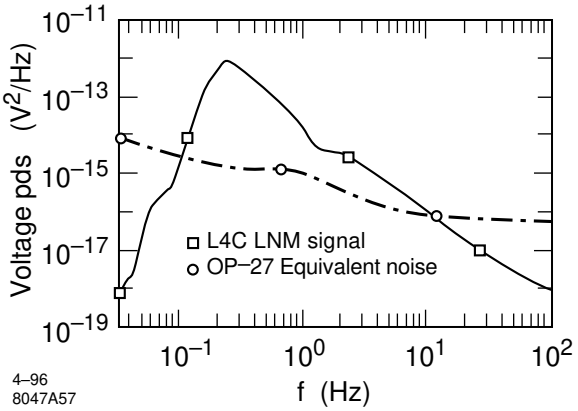


**Figure C-9.** *L4C low-noise model signal and amplifier noise.*

A .707 critically-damped L4C has a total parallel coil+damping resistance of 3.4 kΩ which generates a white-noise spectral density of $5.63 \times 10^{-17}\ \mathrm{V}^2/\mathrm{Hz}$. When integrated over frequencies above one Hz, this contributes noise equivalent to 7-picometer rms motion.

The third and largest source of electronic noise comes from the various amplifiers used with the sensor. Figure C-9 [Rodgers 1992] shows the performance of the L4C with the OP-27 amplifier. The amplifier noise is below the low-noise model signal from about 0.1 Hz to 10 Hz.

## C.3.5 Feedback Seismographs

The most sensitive, low-noise, broad-band modern seismographs employ electromagnetic feedback to stabilize the proof mass to the instrument housing. A model for a feedback seismograph is shown in Figure C-10. Proof-mass motion relative to the instrument housing is detected by a capacitive displacement transducer. This signal is used as the instrument output as well as for feedback control. The feedback elements produce a response equivalent to an oscillator with damping.

The Streckeisen STS-2 is a portable instrument employing feedback to detect seismic signals at the low-noise model level or better from .01 Hz to 10 Hz. Over a wide range of frequencies, the output voltage is proportional to ground velocity $\dot{x}_g$. The instrument contains three identical independent orthogonal seismographs oriented 45° to vertical (Figure C-11). Outputs for vertical and horizontal motions are appropriate vector sums of the three seismograph signals.

To fully model the instrument's response at frequencies around 50 Hz, it is necessary to include the dynamics of the housing's three support legs. The instrument response is the product of the feedback seismograph response and the response of the instrument's support structure. The Laplace transform transfer function for the STS-2 is

$$\frac{V_{\mathrm{out}}(s)}{\dot{x}_g(s)} = \left(\frac{\omega_0^2 + 2\omega_0\zeta s}{s^2 + 2\omega_0\zeta s + \omega_0^2}\right)\left(\frac{Ms^2/k_1C}{\frac{M}{k_1k_2C}s^3 + s^2 + \frac{1}{R_1C}s + \frac{1}{R_2C\tau}}\right) \tag{C.53}$$

and its parameters are listed in Table C-2. The amplitude and phase of this transfer function evaluated with $s = i\omega$ are shown in Figure C-12.

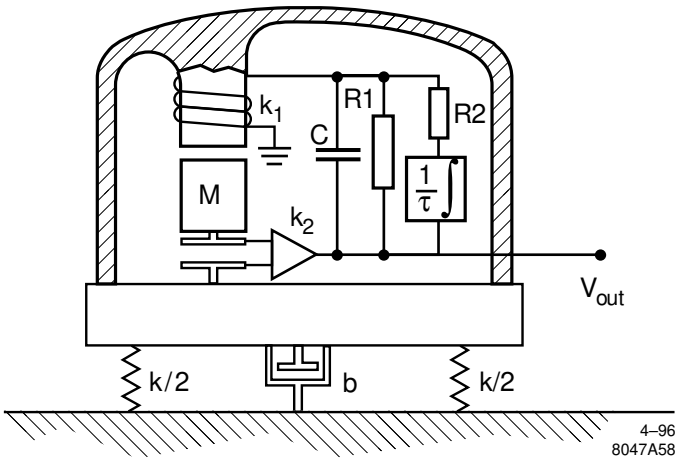


**Figure C-10.** *Feedback seismograph model.*

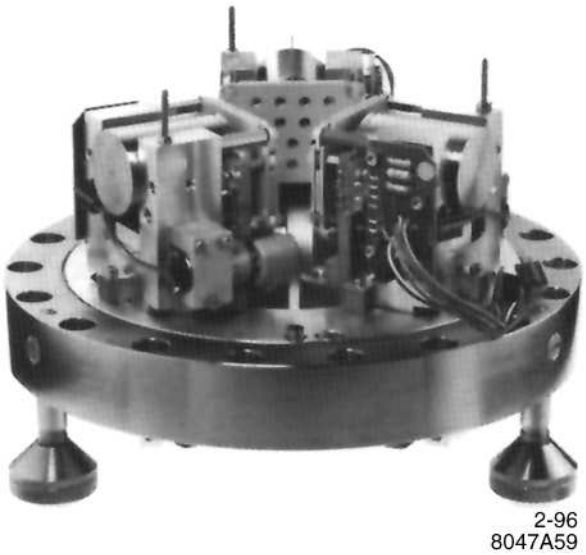


**Figure C-11.** *STS-2 with its cover removed.*

| | | | |
|---|---|---|---|
| Proof mass | $M$ | 0.3 | kg |
| Transduction | $k_1$ | 50 | Newtons/amp |
| Displacement transducer | $k_2$ | $8 \times 10^4$ | V/ m |
| Integration time | $\tau$ | 80 | s |
| Feedback resistor | $R_1$ | $1.7 \times 10^6$ | Ω |
| Integrator resistor | $R_2$ | $0.6 \times 10^6$ | Ω |
| Derivative capacitor | $C$ | $7.8 \times 10^{-6}$ | farads |
| Support frequency | $\omega_0$ | $2\pi(50)$ | rad/s |
| Support damping | $\zeta$ | 0.2 | |

**Table C-2.** *STS-2 parameters.*

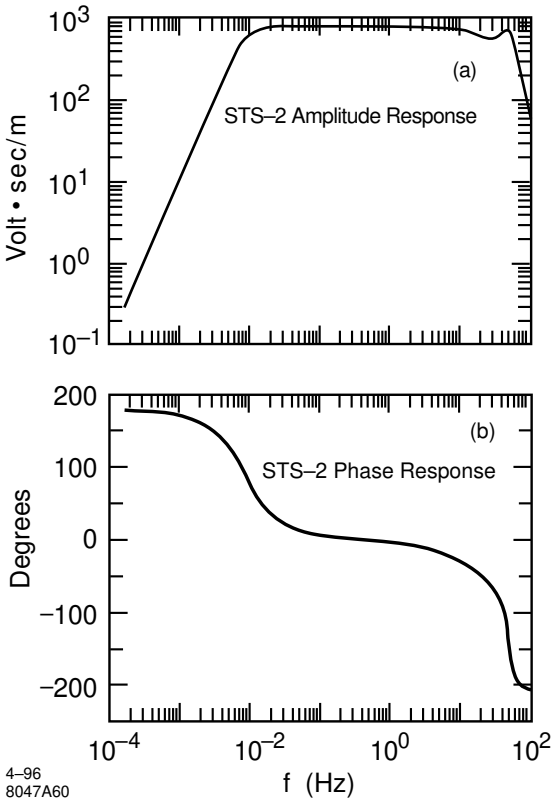


**Figure C-12.** *STS-2 frequency response.*

### C.3.6 Other New Sensors

New methods of measuring inertial forces have recently started development. Optical strain sensor in the form of glass fiber interferometers wrapped around elastic proof-masses have recently been proposed as the basis of a sensitive accelerometer [Gardner 1987]. Field effect tunneling currents are sensitive to Å changes in the tunneling gap. Integrated circuit seismographs have recently been built using tunneling current to monitor proof-mass motion [Kenny 1994]. Because of their small size these instruments are subject to thermal noise but in the future larger transducers using this principle may be developed.

Over the past decade the needs of integrated circuit manufacturing and optical fiber communication have made commercial transducers and actuators available with sub-nanometer resolution. Capacitance position measuring sensors can be purchased with a better than 0.01-nm/$\sqrt{\text{Hz}}$ noise floor and 50-$\mu$m range.

## C.4 SLAC Ground Motion Measurements and Analysis

As discussed in Section C.2, one needs to know both the ground motion spectrum and correlations to compute the its effect on beam motion in the NLC. While much data exists on ground motion spectra,

little is available on its spatial characteristics. One exception is a set of correlation measurements between points separated by 0 to 3 km in the LEP tunnel [Juravlev 1993]. However, the limited resolution of the seismometers used for these measurements does not allow one to fully examine the quantities of interest. To see how typical the CERN results are, and to better understand the dynamics of ground motion, we did a similar set of correlation measurements in the SLAC linac tunnel using higher-resolution seismometers. Because of time constraints, only vertical ground motion was studied in detail. In this section, we describe these measurements, the spectral and spatial analysis of the data, and how the results can be used to compute the effect on beam motion in the NLC.

### C.4.1 STS-2 Measurements and Data Analysis

The seismic measurements were made in the SLAC linac tunnel during a period when the magnet and accelerator cooling water was shut off. Two Streckeisen STS-2 seismometers were borrowed for this purpose and were placed on the tunnel floor with Styrofoam boxes around them for thermal insulation and to shield them from air currents (see Section C.3.5 for a description of these devices). The basic measurement consisted of simultaneously digitizing the vertical ground motion signals from the two seismometers at an effective rate of 128 Hz for about a two-hour period using a PC-based data acquisition system. The actual acquisition rate was 6.4 kHz but the digitized results were decimated by 50 to reduce the data volume to a manageable size. Before decimation, the data were convoluted with a Gaussian function (3 dB point = 96 Hz) to filter out high frequency components.

Over a period of a few weeks, measurements were taken with one seismometer at the end of linac Sector 4, and the other downstream from it by distances ($\Delta$z) of 0, 6, 12, 24, 50, 100, 200, 400, 1000, and 2000 m. After any change in position, the STS-2s were allowed to stabilize for at least 10 hours before data were recorded. Typically, the configuration was kept fixed for one or two days, and three measurements were made each day beginning at 10 PM, 2 AM and 6 AM. The results presented here are based on the 2 AM data.

After completing a measurement, the data were divided into 50 128-s samples and the complex Fourier transform of each sample was computed with a cosine-like windowing function. Since the response function of the seismometers is fairly flat in the frequency ($f$) range of interest, no corrections were applied. However, the seismometers measure velocity, so the Fourier results were divided by $2\pi fi$ to obtain the vertical displacement components, $A_1(f)$ and $A_2(f)$, of the ground motion at the two STS-2 locations. From these, the average of the 50 power spectra were computed, $< A_1^2(f) >$ and $< A_2^2(f) >$, as well as the cross power $< A_1(f)A_2^*(f) >$, from which the correlation was obtained,

$$\text{Correlation} \equiv Re\,\langle A_1(f)A_2^*(f)\rangle \,/\sqrt{\langle A_1^2(f)\rangle\,\langle A_2^2(f)\rangle} \quad . \tag{C.54}$$

Also, the difference spectrum, $\left\langle (A_1(f) - A_2(f))^2 \right\rangle$, was calculated.

### C.4.2 Measurement Resolution

The performance of the measurement system is best characterized by the data that were taken with the seismometers placed side-by-side ($\Delta z = 0$). Figure C-13 shows the two power spectra for this configuration together with the difference spectrum, and the quantity,

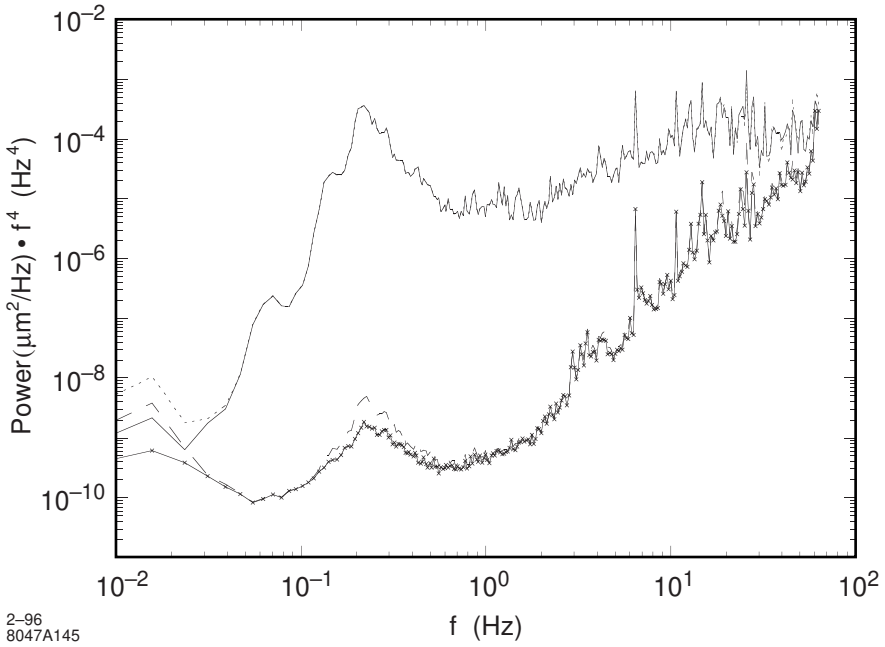


**Figure C-13.** *Vertical power spectra (weighted by $f^4$) measured by two STS-2 seismometers placed side-by-side (solid and dotted lines). Also shown are the difference (dashed line) and corrected difference (line with crosses) power spectra.*

$$\text{Corrected Difference} \equiv 2(1 - \text{Correlation})\sqrt{\langle A_1^2(f)\rangle \langle A_2^2(f)\rangle} \tag{C.55}$$

which would be the difference spectrum if the calibration of the two seismometers were identical and equal to the geometric mean of the actual calibrations (note that the spectra are weighted by $f^4$ to make the plot more compact). One sees that the difference spectrum is generally close to the corrected spectrum except at low frequency where the deviation corresponds to a calibration difference of about a factor of two. Also, the curves deviate near the micro-seismic peak ($f = .2\,\text{Hz}$) where the corresponding calibration difference is only a few parts in a thousand. While this latter deviation is consistent with the expected accuracy of the seismometers, the reason for large low frequency difference is not clear. However it occurs in a region where power spectrum contributes little to the integrated motion so it does not have a big effect on the results.

The difference spectrum in Figure C-13 is roughly that expected from the noise characteristics of the seismometers. To better characterize this noise floor, we computed the integral of the difference spectrum which yields the vertical rms ground motion difference that would be measured if only frequencies above the frequency plotted contributed to the motion. Figure C-14 shows this integrated spectrum together with that for the corrected difference spectrum. Thus, the STS-2s can discern ground motion differences of about 0.5 nm for $f > 0.1\,\text{Hz}$, which is adequate for most NLC studies. As a measure of how sensitive these devices are, we note that this difference level increases by about 100 if the Styrofoam boxes are not used to isolate the seismometers.

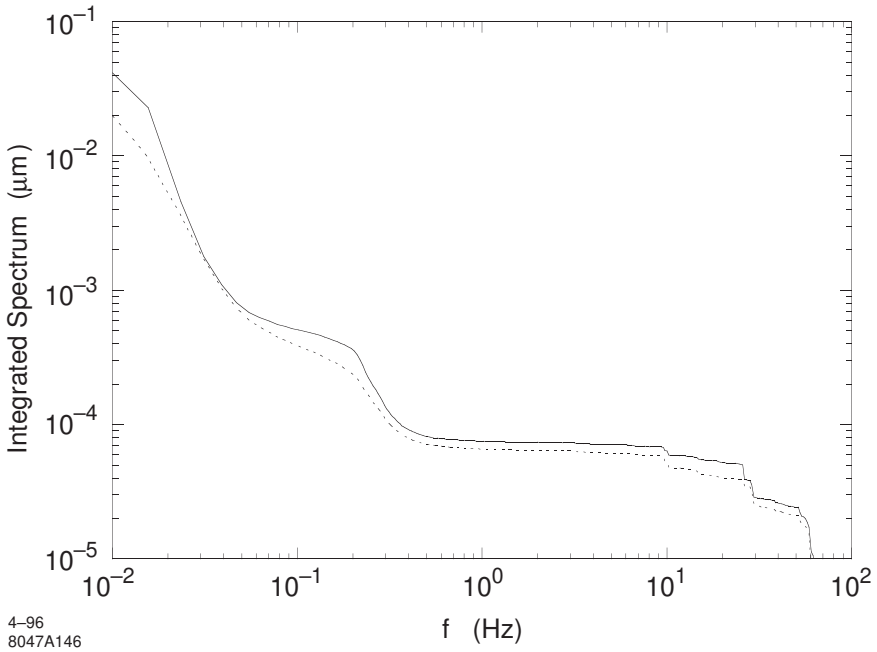


**Figure C-14.** *Integrated difference (solid line) and corrected difference (dotted line) power spectra computed from the difference spectra in Figure C-13.*

### C.4.3 Spatial Properties of the Vertical Ground Motion

The data that were taken with the two seismometers separated by various distances were analyzed in the same manner as described above. One sees that the difference spectra rise as the seismometer separation increases. The differences in these cases are best characterized by the correlation spectra since these ratios tend to be more stable than the power spectra, which can vary by as much as ±10 dB day-to-day. Also, they are more useful for understanding the dynamics of ground motion and for computing its effect on beam transport.

As examples of correlation measurements, Figures C-15 and C-16 show the results obtained with the seismometers separated by 100 m and 1000 m, respectively. As with the CERN results, the correlation is nearly unity at low frequencies (the dip near .01 Hz is due to the electronic noise of the seismometers). Just how the correlation varies with both frequency and separation is needed to compute the effect of ground motion on the beams in the NLC. In examining the data, it was found that it can be reasonably well described by a model in which the ground motion consists of horizontally traveling waves that are isotropically distributed in direction. This model predicts that the correlation equals $J_0(2\pi f \Delta z/v)$ where $J_0$ is the zero order Bessel function, $f$ is the frequency of the waves, $\Delta z$ is the separation of the seismometers, and $v$ is the wave phase velocity, which we find depends on $f$ (*i.e.,* the ground is dispersive).

We determined $v$ as a function of $f$ by dividing the data into narrow frequency bins and then fitting the correlation *vs.* $\Delta z$ curves for each set to the expected Bessel function dependence with velocity as the only free parameter. For this procedure, the log of (1− correlation) was actually fit to better match how the data deviates from unity, which is particularly important for modeling ground motion (note, 1− correlation $= R$ in Section C.2). As an example, Figure C-17 shows the $0.8 < f < 0.9$ Hz data, which have been averaged

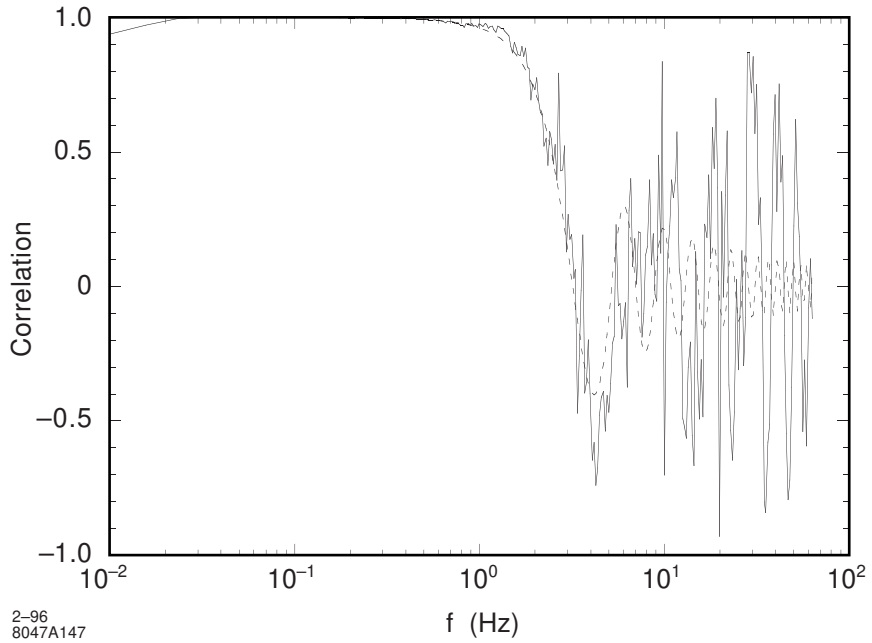


**Figure C-15.** *Correlation spectrum (solid line) measured with the seismometers separated by 100 m. The dashed line is described in the text.*

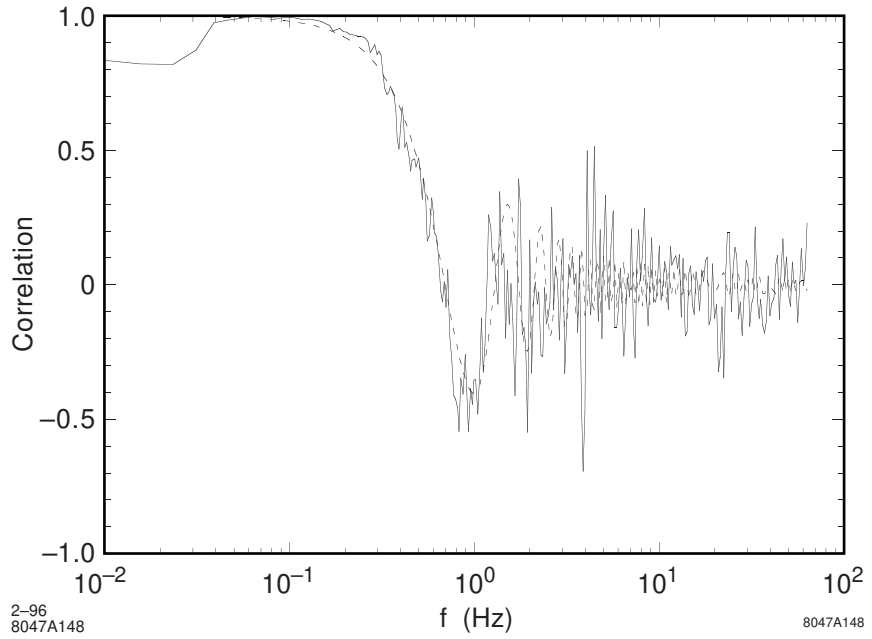


**Figure C-16.** *Correlation spectrum (solid line) measured with the seismometers separated by 1000 m. The dashed line is described in the text.*

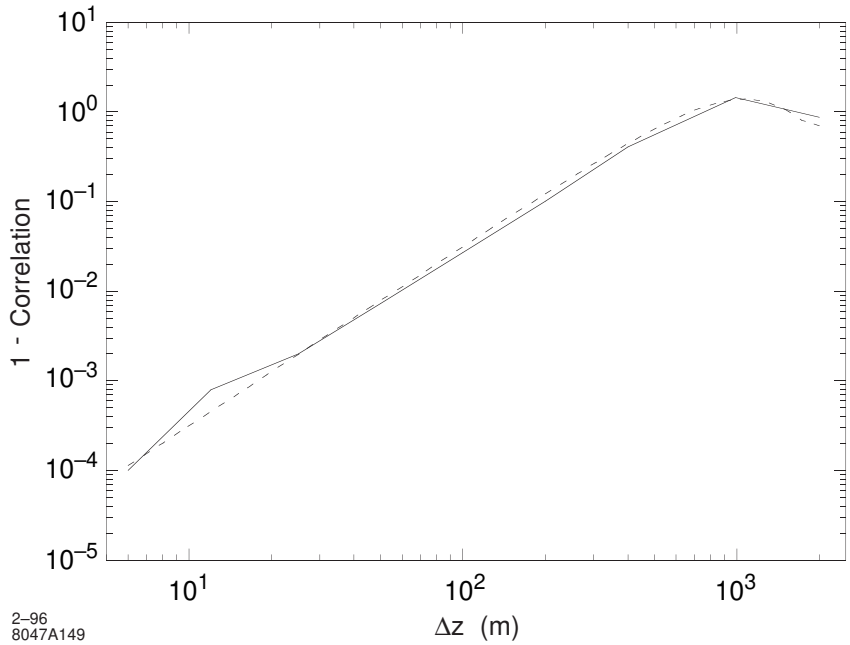


**Figure C-17.** *Dependence of (1− correlation) on the separation ($\Delta z$) of the seismometers for $0.8 < f < 0.9$ Hz. The data in this frequency range has been averaged (solid line). Also shown is the fit to the data (dashed line) which is described in the text.*

together in this plot, and the fit function, $1 - J_0(2\pi f \Delta z/v)$, which is evaluated at the fit velocity, 1510 m/s, and the mean frequency, 0.85 Hz.

The velocity fits were done only for the data in the $0.15 < f < 12$ Hz range. At higher frequencies, the correlations are small even at the lowest values of $\Delta z$ so the velocity dependence is hard to discern. At lower frequencies, the decreasing ratio of ground motion to seismometer noise limits the minimum value of (1− correlation) that can be measured.

The values of velocity that result from the fits are plotted in Figure C-18 as a function of $f$. To characterize the dispersion, the data were empirically fit: an exponential function provides a good match and yields,

$$v(\text{ m/ s}) = 450 + 1900 \exp(-f(\text{ Hz})/2.0) \tag{C.56}$$

which is shown as a dashed line in Figure C-18. To check our results, we have searched geophysics journals for other measurements of dispersion in this frequency range. Although we have not yet found direct measurements, theoretical predictions of the dispersive properties of surface waves at lower frequencies would suggest that our results are not unreasonable [Bolt 1972]. Also, a simple analysis of the CERN data, using only the values of $\Delta z$ at which the correlations first cross zero, yields a similar dispersion relation although the velocities are about 30% larger.

Using the measured dispersion function, the correlation versus frequency measurements were compared to predictions. The dashed lines in Figures C-15 and C-16 are examples. In regions where the correlation is high, the match is good as expected. The fact that the predictions do not match the data in regions of low correlation is less important since it is the $\Delta z$ dependence of transition from high to low correlation that needs to be well modeled to characterize the spatial properties of the ground motion at any frequency.

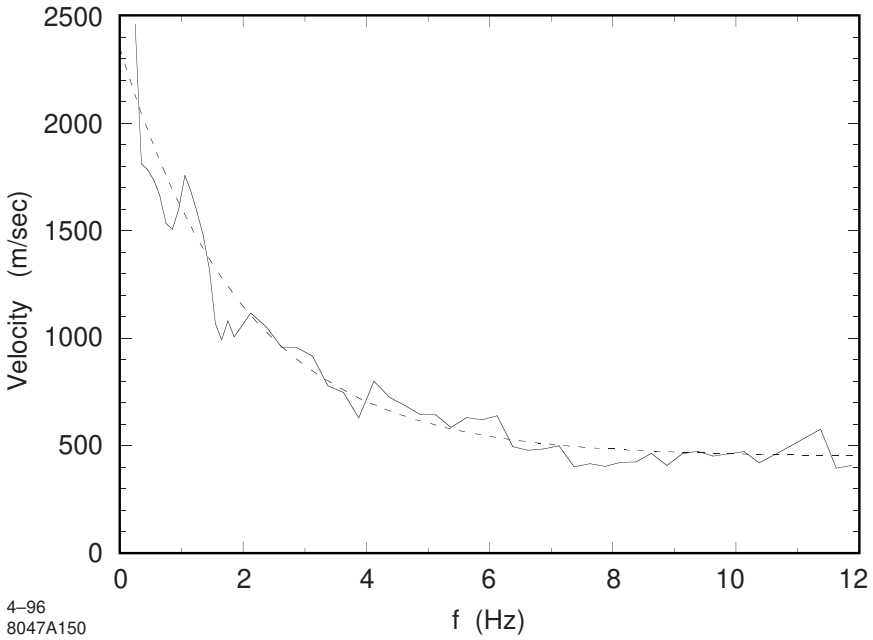


**Figure C-18.** *Velocity derived from fits to the correlation data (solid line). The dashed line is an empirical fit to the data:* $v = 450 + 1900\exp(-f/2.0)$.

So far we have considered only the real part of the measured correlations. If the ground motion is wave-like, and the waves are isotropic in direction, then the imaginary part of the correlations should be zero. What is observed, however, is roughly a $J_1(2\pi f\Delta z/v)$ dependence for frequencies below about 1 Hz. This dependence corresponds to a $(1+\cos(\phi))^2$ distribution of incoming waves where $\phi$ is the angle with respect to the linac axis. This result is not too surprising given that the SLAC linac is oriented nearly perpendicular to the Pacific coastline, and most seismic activity in this frequency range originates from ocean waves. If we redo our analysis of the real component of the correlations assuming a $(1+cos(\phi))^2$ distribution, the velocities that result are systematically about 10% larger, and the goodness-of-fits are about the same. Since only the real part of the correlation is needed for the beam motion predictions, and the $J_0$ dependence adequately matches the data, we continue to use this simple functional dependence and the corresponding dispersion results.

### C.4.4 Application to the NLC

With the correlation function described above, the effect of ground motion on beam transport in the NLC can be derived using the formalism given in Section C.2. In particular, the luminosity reduction, $\Delta\mathcal{L}/\mathcal{L}$, due to vertical ground motion with frequencies $> f_0$ is

$$\Delta\mathcal{L}/\mathcal{L}(f_0) = \frac{\langle\Delta_{\rm IP}^2\rangle_{f_0}}{4\sigma_{y,\rm IP}^2} = \frac{1}{2\pi\sigma_{y,\rm IP}^2}\int_{f_0}^{\infty} P(f)\int_0^{k_0}\frac{G(k)}{\sqrt{k_0^2-k^2}}dk\,df \qquad \text{(C.57)}$$

where: $\sigma_{y,\rm IP}$ = rms vertical beam size at the IP, $k_0 = 2\pi f/v(f)$ with $v(f)$ from Eq. C.56, $P(f)$ = power spectrum, and $G(k)$ = lattice response function, which is defined in Section C.2.2. The effect of trajectory

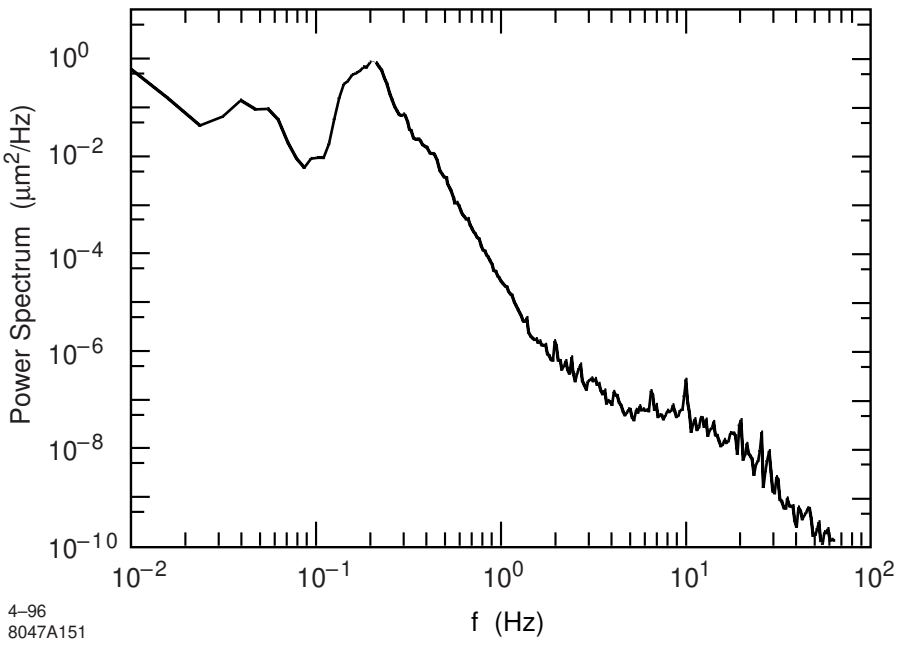


**Figure C-19.** *Average of 10 power spectra of vertical ground motion that were measured on different days in Sector 4 of the SLAC linac at 2 AM.*

feedback loops in the NLC can be included by factoring into the integral the frequency response function of the feedback system.

To a good approximation, one can split the function $G(k)$ for the NLC into a sum over its values in different regions of the machine (this generally yields a worst-case estimate). Only one half of the NLC needs to be considered since $G(k)$ for the opposing half is simply related by symmetry. In this approximation, $G(k)$ for a region is computed for the case where the beam initially follows the ground motion, and the difference in the beam and ground motion that develops by the end of the region remains unchanged relative to the beam size as the beam propagates to the IP. Using the $G(k)$ functions given in Section C.2.2 and the power spectrum that was measured in the SLAC linac tunnel (Figure C-19) and elsewhere, the luminosity losses due to ground motion in most regions of the NLC have been computed.

To be conservative, estimates have also been made which account for the limits that the electronic noise of the seismometers place on our measurement of correlation. As a worst case, the electronic noise contribution to the data is assumed to be ground motion that is uncorrelated, quadrupole-to-quadrupole. That is, at each frequency it is assumed that a certain fraction of the measured power is due to waves, and the remainder is due to uncorrelated motion. Combined, the two sources account for the measured power and correlation spectra except for $\Delta z = 0$ where the predicted correlation is unity but measured is not since the uncorrelated component is actually noise.

The noise power was obtained from the $\Delta z = 0$ difference data and is plotted in Figure C-20 as a fraction ($\equiv \rho_n$) of the average total power (note that $\rho_n$ is the minimum value of (1 - correlation) measurable if the ground motion spectrum equals that in Figure C-19). Including the noise as uncorrelated motion, the

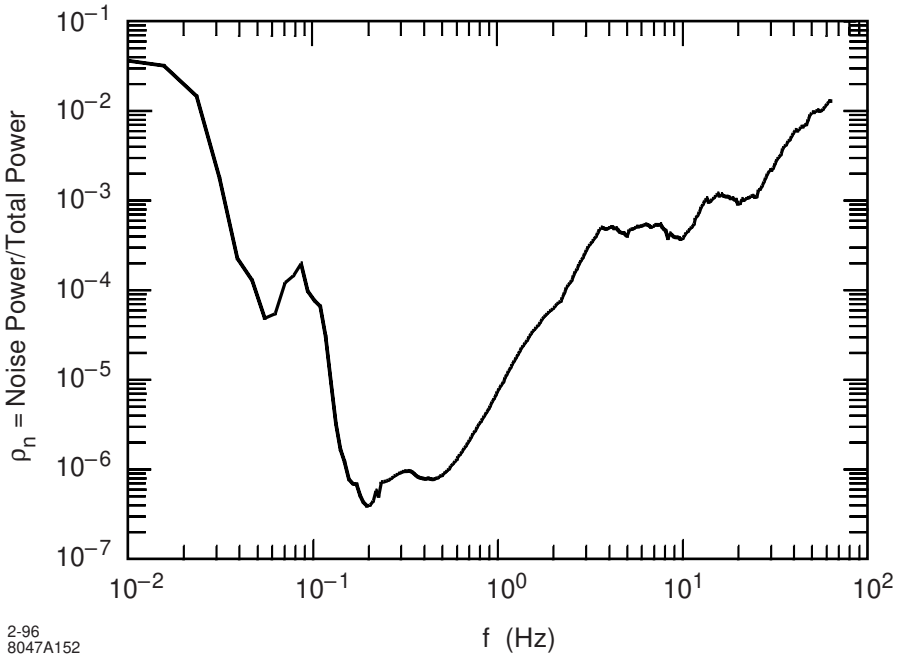


**Figure C-20.** *Fraction ($\rho_n$) of the power in Figure C-19 that is due to STS-2 electronic noise.*

expression for the luminosity reduction becomes

$$\Delta\mathcal{L}/\mathcal{L}(f_0) = \frac{1}{2\pi\sigma_{y,\mathrm{IP}}^2}\int_{f_0}^{\infty} P(f)\left[\int_0^{k_0}\frac{(1-\rho_n)G(k)}{\sqrt{k_0^2-k^2}}dk + \frac{\pi\rho_n G(\infty)}{2}\right]df \quad . \tag{C.58}$$

To predict the luminosity loss due to lower-frequency ($f < .01$ Hz) ground motion requires some assumption about the spatial characteristics of the motion since we do not have measurements in this regime. There is evidence at long time scales (days to years) that ground motion has an "ATL" behavior where the variance of relative displacements grow linearly with time and separation (*i.e.*, $\langle\Delta y^2\rangle = A \times T \times L$ where $A$ is a constant) [Baklakov 1991]. The frequency scale at which the motion changes from predominately wave-like to ATL-like is not known. However, as a worst case, one can assume that this occurs at 0.01 Hz and use the value of $A$ obtained from our data as an upper limit. To compute $A$, we note that the power spectrum for ATL-like motion is

$$P(\omega,k) = 4A/\omega^2k^2 \tag{C.59}$$

so the rms squared difference of the motion for $f > f_0$ at two locations separated by $\Delta z$ is

$$\langle\Delta y^2\rangle = \int_{2\pi f_0}^{\infty}\int_0^{\infty}\frac{4A}{\omega^2k^2}2\left(1-\cos(k\Delta z)\right)\frac{dk}{2\pi}\frac{d\omega}{2\pi} = \frac{A\Delta z}{2\pi^2 f_0} \tag{C.60}$$

For $\Delta z = 200$ m and $f_0 = .02$ Hz, we measure a 10-nm-rms vertical deviation, yielding $A = 2\times10^{-7}\ \mu\mathrm{m}^2/\mathrm{m}/\mathrm{s}$, which is on the low end of that measured on long time scales (another method to compute an upper limit on $A$ is discussed in Section C.2.1). Using this value in the ATL power spectrum above, one can thus

make worst-case estimates of the low frequency contribution to luminosity loss assuming that $A$ is indeed frequency-independent.

The results on luminosity loss due to ground motion in the various regions of the NLC are presented in the chapters that discuss these regions. It should be noted that the general formalism presented here can also be used to estimate beam-emittance growth that depends quadratically on quadrupole position, such as that due to dispersion.

# References

[Baklakov 1991] B.A. Baklakov, P.K. Lebedev, V.V. Parkhomchuk, A.A. Sery, A.I. Sleptsov and V.D. Shiltsev, "Investigation of Seismic Vibrations and Relative Displacement of Linear Collider VLEPP Elements", *Proc. 1991 Part. Accel. Conf.*, San Francisco, CA, 3273 (1991).

[Bolt 1972] B.A. Bolt (editor), "Seismology: Surface Waves and Earth Oscillations", *Methods in Computational Physics*, Vol. 11 (Academic Press, NY, 1972).

[Gardner 1987] D.L. Gardner and S.L. Garret, "Fiber Optic Seismic Sensor", SPIE Vol. 838, *Fiber Optic and Laser Sensors V*, 271–277 (1987),

[Gabrielson 1993] T.B. Gabrielson, "Mechanical-Thermal Noise in Micromachined Acoustic and Vibration Sensors", *IEEE Trans. Electron. Devices* **40**, 903–909 (1993).

[Juravlev 1993] V.M. Juravlev *et al.,* "Investigations of Power and Spatial Correlation Characteristics of Seismic Vibrations in the CERN LEP Tunnel for Linear Collider Studies", CERN Note CERN–SL/93–53 and CLIC–Note 217 (December 1993).

[Kenny 1994] T.W. Kenny, W.J. Kaiser, H.K. Rockstad, J.K. Reynolds, J.A. Podosek, and E.C. Vote, "Wide-Bandwidth Electromechanical Actuators for Tunneling Displacement Transducers", *J. Micro. Elec. Sys.* **3**, 97–103 (1994).

[Riedesel 1990] M.A. Riedesel, R.D. Moore, and J.A. Orcutt, "Limits of Sensitivity of Inertial Seismometers with Velocity Transducers and Electronic Amplifiers", *Bull. Seismological Soc. of Am.* **80**, 1725–1752 (Dec 1990).

[Rodgers 1992] P. Rodgers, "Frequency Limits for Seismometers as Determined from Signal-to-Noise Ratios", *Bull. Seismological Soc. of Am.* **82**, 1071–1098 (April 1992).

## Contributors

- Chris Adolphsen
- Gordon Bowden
- John Irwin